



HAL
open science

COMPARISON OF TWO PURELY EMPIRICAL APPROACHES FOR NON-LINEAR SITE RESPONSE PREDICTION: RESULTS FOR THE ESG6-BLIND TEST (ESG6)

Julie Régnier, Pierre Yves Bard, David Alejandro Castro-Cruz, Boumédiène Derras, Etienne Bertrand

► To cite this version:

Julie Régnier, Pierre Yves Bard, David Alejandro Castro-Cruz, Boumédiène Derras, Etienne Bertrand. COMPARISON OF TWO PURELY EMPIRICAL APPROACHES FOR NON-LINEAR SITE RESPONSE PREDICTION: RESULTS FOR THE ESG6-BLIND TEST (ESG6). The 6th IASPEI / IAEE International Symposium: Effects of Surface Geology on Seismic Motion, Aug 2021, Kyoto (Japan), Japan. hal-04519218

HAL Id: hal-04519218

<https://hal.science/hal-04519218v1>

Submitted on 25 Mar 2024

HAL is a multi-disciplinary open access archive for the deposit and dissemination of scientific research documents, whether they are published or not. The documents may come from teaching and research institutions in France or abroad, or from public or private research centers.

L'archive ouverte pluridisciplinaire **HAL**, est destinée au dépôt et à la diffusion de documents scientifiques de niveau recherche, publiés ou non, émanant des établissements d'enseignement et de recherche français ou étrangers, des laboratoires publics ou privés.

COMPARISON OF TWO PURELY EMPIRICAL APPROACHES FOR NON-LINEAR SITE RESPONSE PREDICTION: RESULTS FOR THE ESG6-BLIND TEST (ESG6)

Régnier Julie¹, Bard Pierre-Yves², Castro-Cruz David³, Boumédiène Derras⁴ and Bertrand Etienne⁵

1 Phd, Cerema, Sophia-Antipolis, France (Julie.regnier@cerema.fr)

2 Researcher, ISterre. Univ. Gustave Eiffel, Grenoble, France (pierre-yves.bard@univ-grenoble-alpes.fr)

3 Phd, Central Supélec, Paris, France (david.castro-cruz@centralesupelec.fr)

4 Professor, Univ-Tlemcen and Univ-Saida, Algeria (boumediene.derras@univ-tlemcen.dz)

5 Phd, Cerema, Sophia-Antipolis, France (Etienne.bertrand@cerema.fr)

ABSTRACT

We use two different purely empirical approaches to estimate the non-linear transfer function between a reference rock and a sedimentary site from recordings of weak ground motions and site-condition proxies (SCPs). The modulus of the linear transfer function is first computed from weak motions and then modulated with a correction to consider non-linear soil behavior. Afterwards, a minimum-phase assumption is used to derive a complex transfer function, which then allows to recover the prediction of acceleration time series $a(t)$ at the sedimentary site.

The first approach uses the non-linear to linear site response ratio RSR_{NL-L} proposed in Derras et al. (2020). This ratio considers both the amplitude changes and the frequency shift between non-linear (strong motion) and linear soil (weak motion) behavior. The data-driven model to predict RSR_{NL-L} is based on various SCPs and ground Motion Intensity Measures (GMIMs). Five SCPs were considered: V_{s30} (time-averaged shear-wave velocity in the top 30 m), $B30$ (vertical velocity gradient in the top 30 m), V_{Smin} (the minimum shear wave velocity), f_0 (the fundamental resonance frequency, picked on H/V ratio) and $A0_{HV}$ (the corresponding peak amplitude), while only one GMIM loading parameter was considered (estimated PGA at KUMA site). In the second approach (Castro-Cruz et al. 2020), the non-linear transfer function is obtained from the linear transfer function (using weak motions recorded at both sites) applying a loading-dependent frequency shift (fsp). The fsp is predicted also using all weaker motion recordings available and the value of the predicted PGA at the sedimentary site.

We apply these two approaches to the material provided for step 3 of the blind prediction exercise organized by the ESG6 Conference. We find that the discrepancy between the two methods was mainly concentrated on the 0.8 to 2 Hz bandwidth for energy content criteria, which is around the linear predominant frequency of the transfer function.

Keywords: empirical prediction, non-linear soil behavior,

INTRODUCTION

The prediction of surface strong ground motions involves many complexities beginning with the seismic source and ending with the propagation of the seismic waves through the very last subsurface soil layers. Close to the surface the seismic waves can be trapped in soft soil layers and the seismic motion at the surface can be amplified compared to rock outcrop sites. These effects called “site effects” differ from site-to-site and event-to-event. In a specific site, the complex site geometry associated with the variability of the incidence of the seismic wavefield can create variability in the site response even for motions having similar amplitudes. Besides, it has been shown that the non-linear soil behavior can significantly modify the site response depending on the incident motion intensity (Pender, 1992; Beresnev & Wen, 1996; Elgamal et al., 2001).

Since then, it has been shown that the non-linear soil behavior will have a different signature in earthquake data depending on type of non-linearity involved. For instance, Bonilla et al., (2005) following the works of Archuleta et al., (2000); Iai et al., (1995); Yu et al., (1993); Zeghal & Elgamal, (1994) showed that saturated dilatant soil can generate spikes in the recorded acceleration due to cyclic mobility and pore water pressure increase during the earthquake. Others showed more classical effects of non-linear behavior that is the decrease of the high- frequency amplitude and the shift of the resonance frequencies to low-frequency bandwidth due to the degradation of the shear modulus and the increase of the damping with shear strain (beginning with Tokimatsu & Midorikawa in 1981). Some researchers also emphasize an increase of amplification at low frequency (Pavlenko & Irikura, 2006; Luis Fabian Bonilla et al., 2011; Kawase, 2006; Régnier et al., 2013, 2016). From previous studies, the non-linear soil behavior may have significant effects on site response and therefore on the acceleration time histories at the surface.

Several approaches can be used to predict the strong ground motion at the surface. Numerical simulations of wave propagation require the definition and calibration of a soil model including a constitutive soil model, which can be challenging to define. When earthquake recordings at the prediction site are available, the use of empirical approaches based on such recordings may be considered, such as for instance the empirical Green's function technique, provided some constraints on source location and mechanism (e.g. Irikura, 1986). For now however, the non-linear soil behavior is not considered accounted for in classical EGF approach. When recordings of previous earthquakes are simultaneously available at the prediction site and at near-by reference site, pure empirical approaches can be used that do consider the non-linear soil behavior (Castro-Cruz et al., 2020; Derras et al., 2020). The purpose of this paper is to test and compare these last empirical approaches on the ESG6 blind prediction data.

PRESENTATION OF THE PURE EMPIRICAL METHODS

Methodology to obtain a non-linear prediction from linear site response:

We are using two purely empirical approaches to predict the surface acceleration time histories and the associated Fourier spectrum for both the foreshock and the mainshock of the Kumamoto 2016 earthquake. Both methods use statistically defined correction factors that are applied to the site-specific linear transfer function to account for the non-linear soil behavior.

1. The linear transfer function (TF_{lin}) can be obtained from weak ground motions recordings or numerical simulations, it can be borehole or outcrop transfer function. In this paper, we use the weak motions recorded at the reference rock site SEVO and at the target sedimentary site KUMA.
2. The non-linear transfer function (TF_{NL}) is corrected for the non-linear soil behavior as follows:

- a. The first method (Method 1) defines a function so-called RSR_{NL-L} that is to be multiplied by the TF_{lin} to define the modulus of the non-linear transfer function (TF_{NL}) between SEVO and KUMA according to eq 1

$$TF_{NL}(f) = TF_{lin}(f) \cdot RSR_{NL-L}(f) \quad (\text{eq. 1})$$

- b. The second method (Method 2), defines a parameter so-called fsp (frequency shift parameter). This, shift the linear transfer function according to the equation 2.

$$TF_{NL}(f) = TF_{lin}(f/\sqrt{fsp}) \quad (\text{eq. 2})$$

3. Then a minimum phase assumption allows to associate a realistic phase to the modulus of the non-linear transfer function TF_{NL} , and obtain a complex transfer function
4. This complex transfer function is then applied to the Fourier transform of the acceleration time histories recorded at SEVO (derived from the velocity recordings), and an inverse Fourier transform provides the predicted acceleration time histories at KUMA

Details on the correction factors

First method: Correction for soil non-linear behavior using RSR_{NL-L} :

The approach is based on the work of Derras et al. (2020), which predicts a linear to non-linear correction curve, called RSR_{NL-L}, to correct both the amplitude changes and the frequency shift associated to the non-linear soil behavior, with respect to the modulus of the linear transfer function derived from weak motion recordings at both KUMA and SEVO.

This correction function is estimated on the basis of a statistical analysis of a selection of KiK-net recordings, which were used to train an artificial neural network (ANN) in order to predict the frequency-dependent correction function RSR_{NL-L} as a function of one ground motion intensity measure (GMIM), site-condition proxies (SCPs). The ANN approach was inspired by investigations into the human brain structure, which consists of interconnected neurons. An ANN is made up of input, hidden and output layers, and the connections between neurons of two consecutive layers are characterized by linear combinations of inputs: the corresponding synaptic weights (W) and biases (b) are the learnable parameters of a ANN. The W values characterize the influence of input (GMIM, SCPs) on the output (RSR_{NL-L}). The Quasi-Newton Back Propagation technique also called "BFGS" (Robitaille et al., 1996) has been used in this work for the training phase. To avoid the overfitting, the regularization method presented in (Derras et al., 2012) is used in this study. More details upon the structure and the design of ANN can be found in Derras et al. (2020).

The performances of the ANN results are measured by the standard deviation of residuals between observations and model predictions, compared to the standard deviation of the original advanced data set through the variance reduction coefficient R_c (Derras et al., 2017) as defined in eq. 3

$$R_c = \left[1 - \frac{\left[\sqrt{\frac{1}{M} \sum_1^M \left(\log_{10}(RSR_{NL-L,obs}) - \log_{10}(RSR_{NL-L,pred}) \right)^2} \right]^2}{\left[\sqrt{\frac{1}{M} \sum_1^M \left(\log_{10}(RSR_{NL-L,obs}) - \log_{10}(\text{mean}(RSR_{NL-L,pred})) \right)^2} \right]^2} \right] \cdot 100 (\%)$$

eq. 3

Where RSR_{NL-L,obs} represents the "observed" RSR_{NL-L} as derived in the step 3 advanced data set. RSR_{NL-L,pred} is the neural prediction of the RSR_{NL-L}. This function is predicted either in the normalized frequency domain with a frequency parameter called f_{NL} defined in (Régnier et al., 2016) for the sensitivity study, or in the absolute frequency domain for the final model). M is the size of the data set.

The final neural models thus consist of a series of three layers. The first represents N inputs, (one GMIM and {N-1} SCPs). Here, N=6 (5 SCPs and 1 GMIM, PGA). The second, hidden layer has the same number N of neurons. The last layer represents the values of RSR_{NL-L} for 49 absolute frequency bins. The selected architecture is therefore of the N-N-97 or N-N-49 type.

The model chosen in this article to predict RSR_{NL-L} is based on site parameters V_{s30} (mean shear Vs over the first 30 m), B_{30} (gradient of the velocity profile over the first 30 m), V_{smin} (the minimum shear wave velocity), f_0 (the fundamental resonance frequency, picked on H/V ratio), and A_{0HV} (the corresponding peak amplitude), and on a loading parameter characterizing the intensity of ground shaking at KUMA (GMIM) site, here PGA. Whereas in Derras et al., 2020, we have used two SCPs (V_{s30} and f_{0HV}) and PGV/V_{s30} to represent the GMIM (03 neurons at the hidden layer).

Second method : Correction for soil non-linear behavior using fsp

Castro-Cruz et al. (2020) used a subset of the KiK-net database to define the fsp parameter. This subset is composed of 688 stations. Among them, 650 sites are characterized with Vs and Vp profiles, soil description, and information on the stations (location and information of recording devices. For each recording, the acceleration time histories are provided, with the event origin time, the epicenter location, the depth of the hypocenter, and the magnitude of the event determined by the Japanese Meteorological

Agency (JMA). Recordings were selected according to two criteria: signals from earthquakes with a magnitude higher than 3 and with an epicentral distance lower than 500 km. These two criteria lead to 75 232 pairs of 3-components signals (surface and downhole) from 5535 events with magnitudes between 3 and 9, recorded between November 1997 to December 2017. For all of the selected seismograms the weak ground motions corresponding to assumed linear behavior are selected based on their maximal peak accelerations ($PGA_{downhole}$ from 10^{-4} m/s² to $6 \cdot 10^{-3}$ m/s² are considered). The linear Borehole Spectral Ratio (BSR_{lin}) is the arithmetic average of all of the weak ground motions BSR. It is compared to each BSR_{NL} from all stronger ground motions recorded at the same site, allowing us to define a parameter that characterizes the observed frequency shift. The logarithmic frequency shift is the gap in logarithmic scale between BSR_{lin} and BSR_{NL} . In linear scale, it is a coefficient that changes the frequency scale. The algorithm to find this logarithmic shift minimizes the misfit between BSR_{lin} and BSR_{NL} as defined in Equation (2). Note that the misfit is weighted by the logarithmic sampling.

$$misfit = \sum_i \left| BSR_{lin} \left(\frac{\bar{f}}{Ls} \right) - BSR_{NL}(\bar{f}) \right| \Delta x$$

$$\Delta x = \log_{10} \left(\frac{f_{i+1}}{f_i} \right)$$

$$\bar{f} = 0.5(f_{i+1} + f_i)$$

eq. 4

In Eq. 4, Ls is the frequency scaling factor applied to BSR_{lin} . The misfit is defined as a discrete approximation of the area between the shifted BSR_{lin} and BSR , considering a logarithmic scale as the length of the base (Δx). The computation is done over a frequency window going from 0.3 Hz to 30 Hz.

Finally, we define a frequency shift parameter, so called fsp , as the square of the Ls , which produces the minimum value of misfit ($fsp=Ls^2$ when misfit is minimized).

In the equivalent linear approximation (EQL), the nonlinearity of the soil behavior is taken into account in an iterative process that adjusts the elastic properties to the level of strain induced in the layer, knowing both the modulus reduction and the attenuation curves. In this frame, the shear modulus at a linear strain rate (G_{max}) can be compared to the shear modulus at larger strain (G), by the ratio between both. Using Equation (4) for both modulus, the ratio will be expressed as followed:

$$\frac{G}{G_{max}} = \left(\frac{f}{f_{lin}} \right)^2 = fsp$$

eq. 5

Equation (5) shows that the ratio of the shear modulus is proportional to the square root of the ratio between the linear resonance frequency f_{lin} and the non-linear ones (whatever the order of the harmonic). In logarithmic scale, this ratio (f/f_{lin}) represents a logarithmic shift it is the definition of the fsp parameter. Therefore, in a 1-D monolayer case, the shear modulus reduction is equal to the previously defined fsp .

RESULTS

Definition of the RSR_{lin}

TF_{lin} is the average of the weak motion ratio between the Fourier spectrum of the velocity recorded at KUMA and SEVO. To obtain the horizontal transfer function we used the average between the two horizontal components. The vertical transfer function was obtained using the vertical Fourier spectrum ratio.

The accelerometric data were pre-processed following the recommendations of Boore and Bommer (2005). From the acceleration time histories at KUMA, we integrated the signal to obtain the velocity time histories. Before performing the integration, we apply pre-processing that includes removing the mean, the tapering, the addition of zeroes before and after the signal, and a 2-poles butterworth filtering between 0.1 and 30 Hz. The Fourier spectra were calculated and smoothed using a Konno-Ohmachi smoothing (Konno & Ohmachi, 1998) with a parameter of 40. The average and standard deviation of the RSR_{lin} are illustrated in Figure 1. We also calculated the H/V at the surface (red curves) and the

numerical transfer function (in blue curve) using the preferred soil models provided by the organizing team.

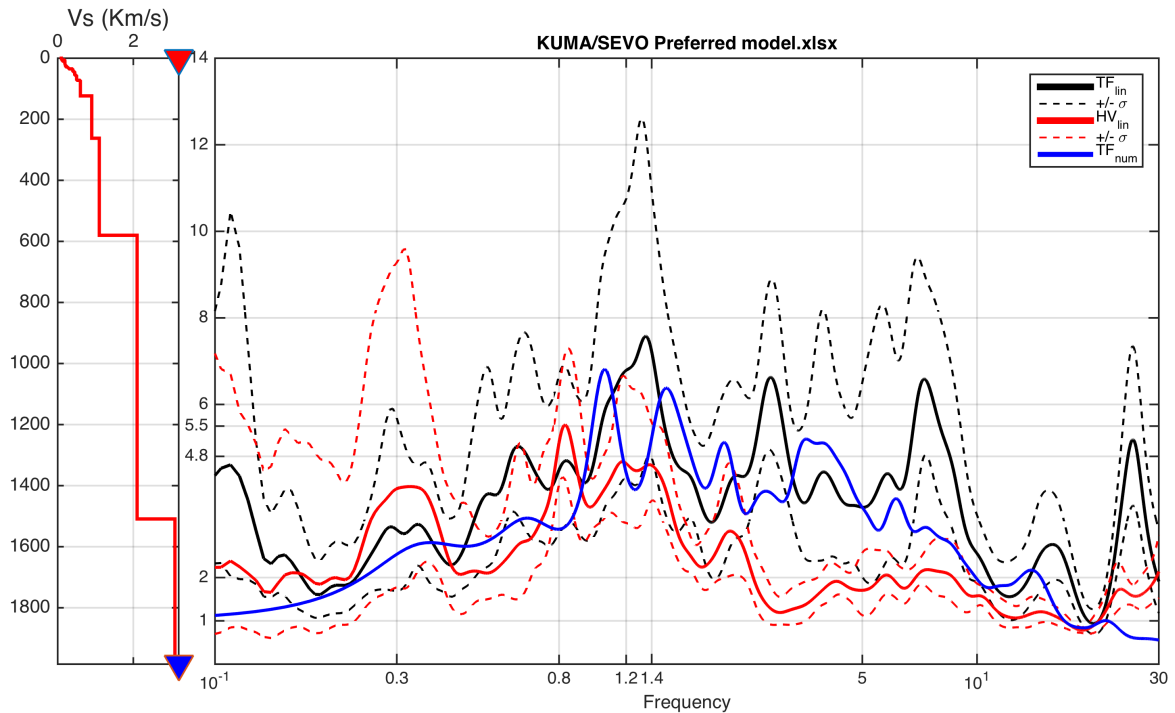


Figure 1: Left : Vs profile at KUMA site (left). Right: comparison of the linear spectral ratio between KUMA and SEVO velocity time histories (geometrical average TF_{lin} and average ± 1 standard deviation, black), H/V at Kuma site (average HV_{lin} and average ± 1 standard deviation, red) and the 1-D linear numerical outcrop transfer function (TF_{num} , blue)..

Required site (SCPs) and input motion (GMIMs) parameters

The values of the site parameters were derived from the preferred soil model proposed by the organization and illustrated in figure 1. We also tested the Vs profiles provided in the first round of the benchmark by Diego Mercerat and Cécile Cornou but a sensitivity study showed that the predictions of non-linear corrections factors are very robust whatever the velocity model derived for the KUMA site. The fundamental resonance frequency f_0 (Hz) was obtained from the empirical site response curves and confirmed by the H/V spectral ratio.

Table 1: KUMA site parameters (SCPs) used for the prediction of NL correction

V_{S30} (m/s)	B_{30}	f_0 (Hz)	V_{Smin} (m/s)	A_{OHV}
160	0.3	0.3	95	4.8

The PGA of the foreshock and mainshock were predicted using the linear regression between the log10 of PGA_{KUMA}/PGA_{SEVO} modulated by the ratio between epicentral distance at KUMA and SEVO ($Depi_{KUMA}/Depi_{SEVO}$). The predicted PGA is 2.36 m/s^2 for the foreshock and 4.85 m/s^2 for the main shock. However, after a first round of calculation, we found a PGA for the foreshock at KUMA around 4.12 m/s^2 , we decided to update the calculation using this value to correct for the non-linear soil behavior.

Corrections factors and RSR_{NL}

First method : Correction for soil non-linear behavior using RSR_{NL-L} :

To predict the correction factor for the nonlinearity, we used the site parameters defined in Table 1 and the PGA predicted at KUMA. Such a set of parameters is not the one that performs the best in terms of variance reduction, but it is a good compromise between ease of use (knowing the velocity profile) and model performance: the corresponding standard deviation reduction (R_c) is 18%.

The use of the additional parameter f_{NL} , that is a frequency from which we observe a de-amplification in the site response, would have increased R_c to 25%. However, in this case, considering that no other large events were recorded at KUMA and SEVO sites, it would have been necessary to infer a value for f_{NL} from f_{0HV} , and such a derivation is associated with a large uncertainty.

Figure 2 displays the so-obtained RSR_{NL-L} curves for the foreshock and the mainshock. Both curves are very closed since the predicted PGA at KUMA are very close. Below 1.2Hz, the non-linear soil behavior results in a slight increase of the amplification (around 10%), and above this frequency in a significant decrease that exceeds 40% between 10 and 20 Hz. As expected, the impact of non-linear soil behavior is slightly more important for the mainshock (dashed line).

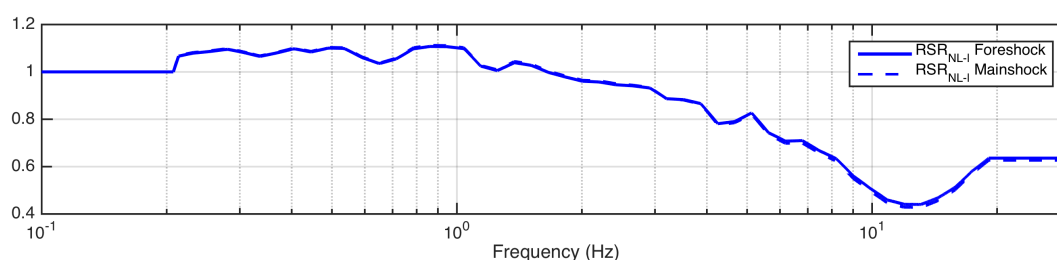


Figure 2: Correction curves for the foreshock and the mainshock.

Second method : Correction for soil non-linear behavior using f_{sp}

Following the procedure described in Castro-Cruz et al. (2020), we obtain the frequency shift for each RSR with respect RSR_{lin} . The f_{sp} is then plotted in function of the intensity of the ground motions (see Figure 3). Using a non-linear correlation between the f_{sp} and the intensity parameter (here the PGV at SEVO), we predict the f_{sp} for the two strongest events. The red vertical lines in Figure 3 represent the PGV recorded at SEVO for the two target events. One can notice that the shift predicted differs depending on the component and considering that there is only weak motion data, the prediction is not constrained for the PGV recorded at SEVO for the foreshock and the main event.

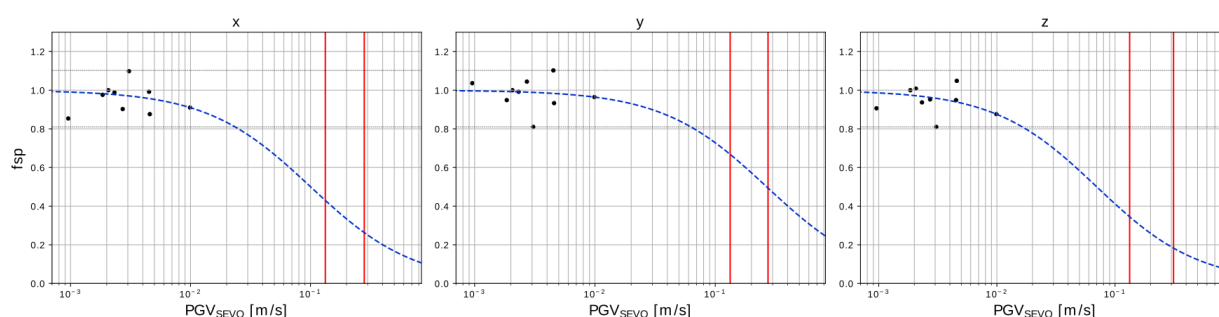


Figure 3: f_{sp} curves for the three directions, NS (x), EW (y).

Comparison of results

Transfer function

Figure 4 illustrates the transfer functions predicted by the two methods for the two events. The first method modifies mainly the amplitude of the transfer function, while the second method applies only a shift of the resonance frequencies. For the second method, the shape of the transfer function is different from the linear one, this is due to the fact that a different shift is applied to each horizontal component of the transfer function. In the following figure, the average between horizontal components of the transfer function is illustrated.

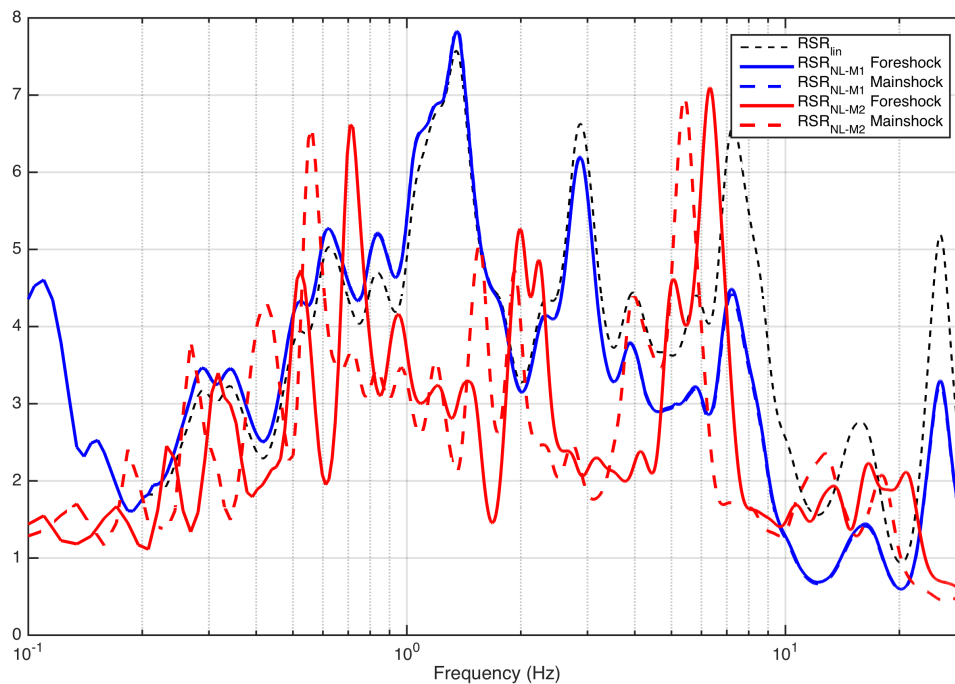


Figure 4: Comparison of the transfer functions (average on the two horizontal components) corrected by the two methods with the linear transfer function for the foreshock and the mainshock.

Fourier Spectrum at the surface

The predicted Fourier spectra using a linear transfer function and the two non-linear transfer functions corrected with the methods 1 and 2 at the KUMA surface site are compared in Figure 5. This comparison is made for the three components of motion (as one can notice, in the first method the vertical component is not corrected for non-linear soil behavior) of the foreshock (Ev 1) and the mainshock (Ev 2). We can observe that the main effect of the first method – as expected from Figure 3 - is a decrease of the Fourier spectra amplitude at high frequencies, while the second method exhibits larger discrepancies with the linear prediction with a clear shift of the frequencies to the low frequency bandwidth. Whatever the method used the Fourier spectra at SEVO is amplified over a broad frequency range (at least 0.3 - 10 Hz). For the vertical component, the linear and the non-linear Fourier spectrum are similar for the first method.

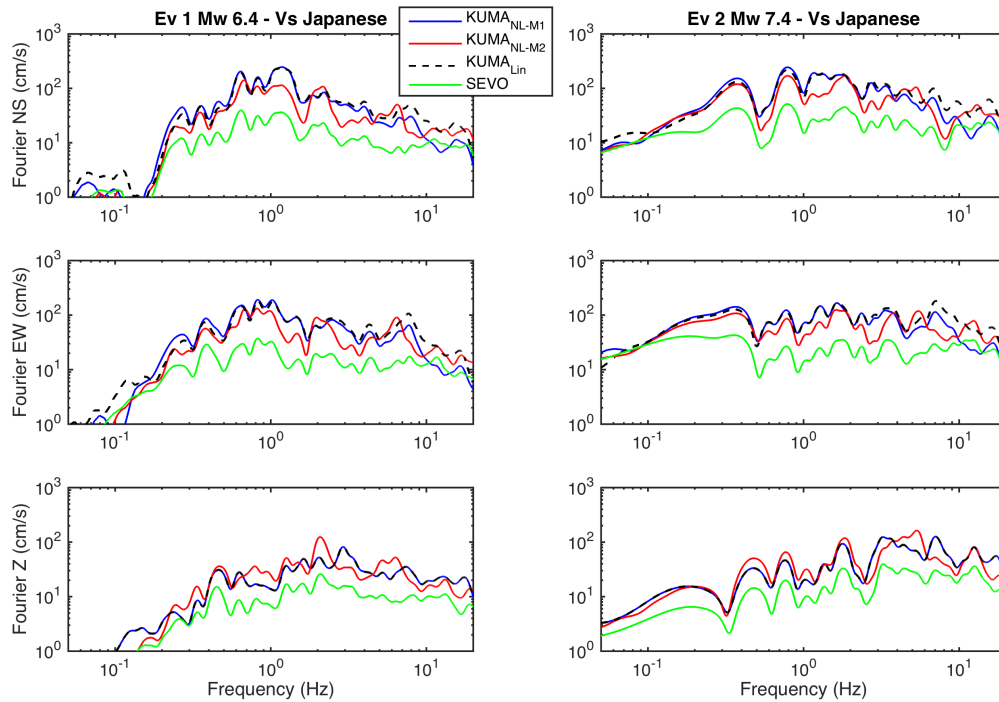


Figure 5: Fourier spectra at the surface of the predicted earthquake at Kuma using only the linear transfer function and the non-linear transfer function corrected by the two methods. The Fourier spectra at SEVO is also provided as a reference.

Acceleration time histories at KUMA surface site

The time domain predictions displayed for two time windows (14-21s in Figure 6 and 21-26 s or 21-24 s in Figure 7) indicate similar overall waveforms, with however very significant amplitude changes. The similarity is due to the minimum phase assumption for all predictions. The frequency shift correction of the second method makes the accelerations at a specific time either increased or decreased, while the first method systematically provides results with lower amplitude than the linear one (except for the vertical component where method 1 assumes a linear site response).

The predicted PGA values were 4.12 m/s^2 for the foreshock and 4.85 m/s^2 for the main shock, in the following figures we can observe that the predicted PGA are 3.9 and 4.9 m/s^2 for the first method which is equivalent to the predicted ones.

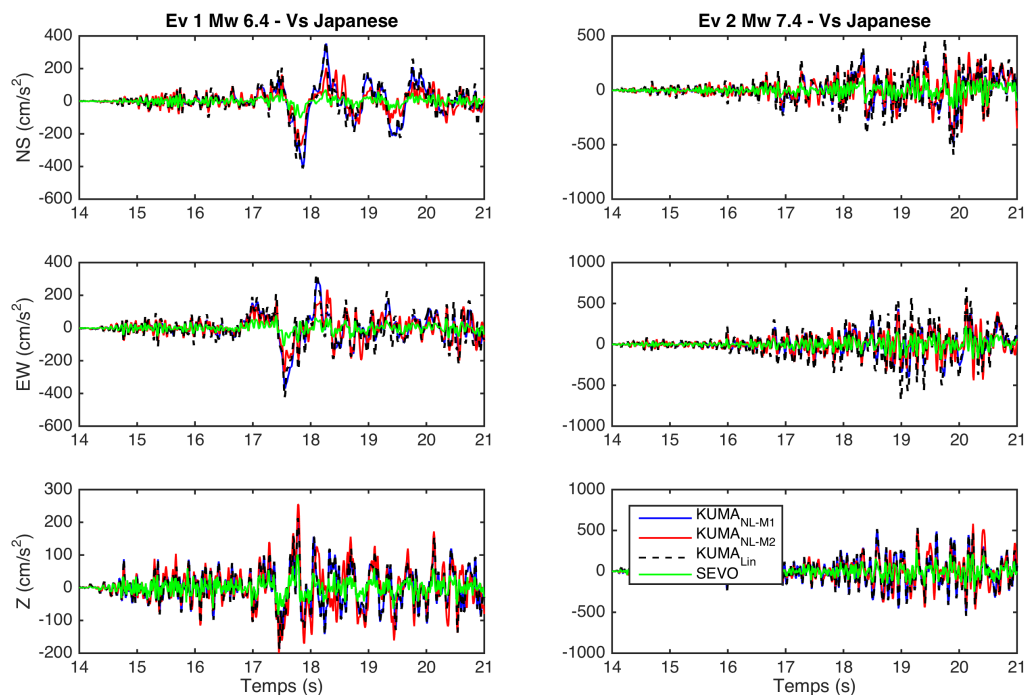


Figure 6: Acceleration time histories at the surface of the predicted earthquake at Kuma using only the linear transfer function and the non-linear transfer function corrected by the two methods. The acceleration at SEVO is also provided as a reference. Zoom between 14 to 21 seconds.

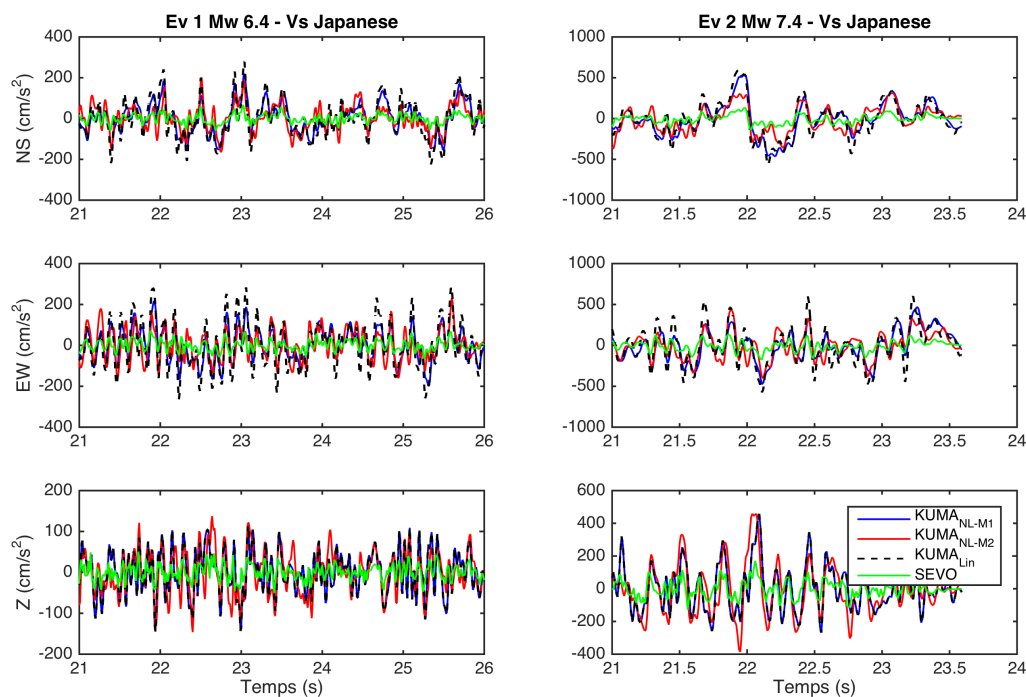


Figure 7: Zoom between 21 to 26 seconds for the foreshock.

Quantifying the differences with Anderson goodness-of-fit criteria

The two sets of predictions can be compared in a more quantitative way using some "goodness-of-fit" measures. In that aim, the 10 criteria proposed by Anderson (2004) are considered here, labeled as SDA for Arias duration, SDe for Energy duration, Sia for Arias Intensity, Siv for Energy Integral, Spga for

PGA, Spgv for PGV, Spgd for PGD, Ssa for response spectra and finally Sf for Fourier spectra. For instance, for the PGA parameter, the Anderson goodness-of-fit is estimated by the Eq.6, where PGA_1 and PGA_2 are the PGA values predicted by the first and de second method.

$$S(PGA_1, PGA_2) = 10. \exp \left[- \left(\frac{PGA_1 - PGA_2}{\min(PGA_1, PGA_2)} \right)^2 \right]$$

Eq.6

Given this formula, a GOF score from 8 to 10 is considered an excellent fit, from 6 to 8 a good fit, from 4 to 6 a medium fit and below 4 a poor fit.

Figure 8 diagrams indicate very high scores for frequencies above 2 Hz, and lower scores at lower frequencies, especially for the energy content (Sla and Siv) in the frequency range corresponding to largest amplifications, i.e., between 0.8 to 2 Hz. This result is in good agreement with the comparison of the predicted transfer function from M1 and M2 where the shift performed in the second method creates a trough in this specific frequency range. Comparing the results from the 2 events, it is surprising to observe that the discrepancy between the two methods is more pronounced for the first event where less non-linear behavior is observed.

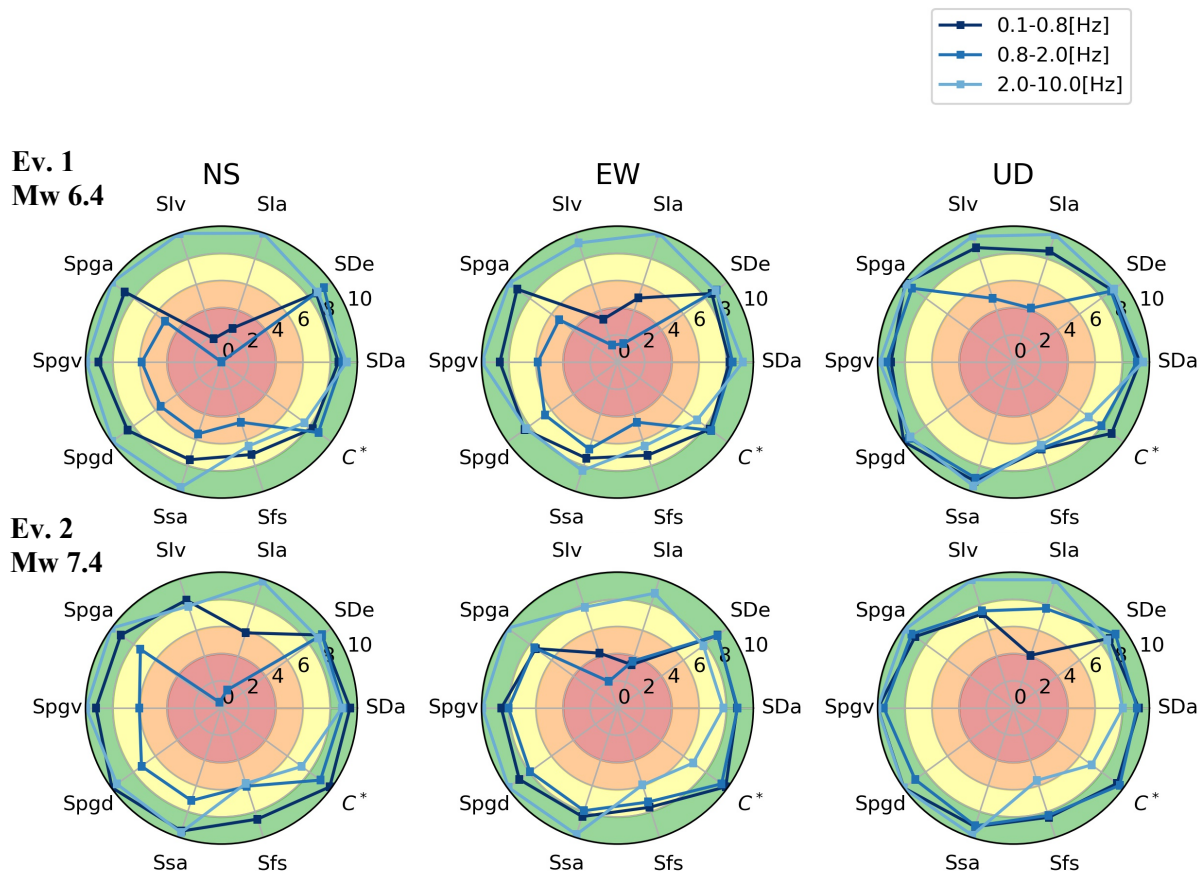


Figure 8: Anderson criteria of goodness of fit between the surface acceleration predicted by the method M1 and the method M2.

CONCLUSIONS

These two purely empirical approaches provide acceleration time histories predictions which differ significantly from one another. The first method involves a simple modulation for the linear amplification curve, combining a slight increase at low frequencies, and a significant decrease at high frequencies, reproducing the two main observations of non-linear behavior on site response, i.e., the shift of the resonance frequency towards lower values, and the amplification decrease associated to increase of soil damping with larger strain. The second method emphasizes the first aspect of soil non-

linear behavior with a shift of the whole linear transfer function. The results are compared in terms of Fourier spectrum, non-linear transfer function, acceleration time series and Anderson criteria.

The main differences between the two approaches are found between 0.8 Hz (1.25 s) and 2 Hz (0.5 s), which corresponds to the frequency range with largest linear amplifications (predominant frequency), and mainly affect the energy content parameters. One of the next step is to perform an iterative correction of the non-linear soil behaviour until we reach an agreement between the PGA use to define the non-linear corrections and the predicted ones.

Finally, only with the comparison of the results with the real recording at KUMA site will it be possible to provide more definitive conclusions on the validity of each method, and may be to develop a hybrid approach to predict strong ground motion including non-linear soil behavior.

AKNOWLEDGEMENTS

We would like to thanks all the organizing team of the ESG6 blind test for setting up this benchmark.

REFERENCES

- Anderson, J. G. (2004). Quantitative measure of the goodness-of-fit of synthetic seismograms. *13th World Conference on Earthquake Engineering*, 243.
- Archuleta, R. J., Steidl, J. H., & Bonilla, L. F. (2000). Engineering insights from data recorded on vertical arrays. *Proc.*
- Beresnev, I. A., & Wen, K. L. (1996). Nonlinear soil response, A reality? *Bulletin of the Seismological Society of America*, 86(6), 1964–1978.
- Bonilla, Luis F., Archuleta, R. J., & Lavallée, D. (2005). Hysteretic and Dilatant Behavior of Cohesionless Soils and Their Effects on Nonlinear Site Response: Field Data Observations and Modeling. *Bulletin of the Seismological Society of America*, 95(6), 2373–2395.
- Bonilla, Luis Fabian, Tsuda, K., Pulido, N., Regnier, J., & Laurendeau, A. (2011). Nonlinear site response evidence of K-net and KiK-net records from the Mw 9 Tohoku earthquake. *Earth Planets Space*, 58.
- Boore, D. M., & Bommer, J. J. (2005). Processing of strong-motion accelerograms: Needs, options and consequences. *Soil Dynamics and Earthquake Engineering*, 25(2), 93–115.
- Castro-Cruz, D., Régnier, J., Bertrand, E., & Courboulex, F. (2020). A new parameter to empirically describe and predict the non-linear seismic response of sites derived from the analysis of Kik-Net database. *Soil Dynamics and Earthquake Engineering*, 128, 105833.
- Derras, B., Bard, P.-Y., & Cotton, F. (2017). V S30, slope, H 800 and f 0: Performance of various site-condition proxies in reducing ground-motion aleatory variability and predicting nonlinear site response. *Earth, Planets and Space*, 69(1), 1–21.
- Derras, B., Bard, P.-Y., Cotton, F., & Bekkouche, A. (2012). Adapting the Neural Network Approach to PGA Prediction: An Example Based on the KiK-net Data. *Bulletin of the Seismological Society of America*, 102(4), 1446–1461.
- Derras, B., Bard, P.-Y., Régnier, J., & Cadet, H. (2020). Non-linear modulation of site response: Sensitivity to various surface ground-motion intensity measures and site-condition proxies using a neural network approach. *Engineering Geology*, 269, 105500.
- Elgamal, A., Lai, T., Yang, Z., & He, L. (2001). *Dynamic soil properties, seismic downhole arrays and applications in practice*.
- Iai, S., Morita, T., Kameoka, T., Matsungaya, Y., & Abiko, K. (1995). Response of a dense sand deposit during 1993 Kushiro-Oki earthquake. *Soils and Foundations*, 35(1), 115–131.
- Irikura, K. (1986). Prediction of strong acceleration motion using empirical Green's function. *Proc. 7th Japan Earthq. Eng. Symp*, 151–156. http://basin.earth.ncu.edu.tw/download/courses/seminar_MSc/2011/1006-1_01.pdf
- Kawase, H. (2006). Site effects derived from spectral inversion method for K-NET, Kik-net and JMA Strong-motion Network with special reference to soil nonlinearity in high PGA records. *Bulletin of Earthquake Research*, 81, 309–315.
- Konno, K., & Ohmachi, T. (1998). Ground-motion characteristics estimated from spectral ratio between horizontal and vertical components of microtremor. *Bulletin of the Seismological Society of America*, 88, 228–241.
- Pavlenko, O. V., & Irikura, K. (2006). Nonlinear Behavior of Soils Revealed from the Records of the 2000 Tottori, Japan, Earthquake at Stations of the Digital Strong-Motion Network Kik-Net. *Bulletin of the Seismological Society of America*, 96(6), 2131–2145.
- Pender, M. J. (n.d.). Linear and nonlinear earthquake site response. In *Predictive soil mechanics* (pp. 529–543). <https://www.icevirtuallibrary.com/doi/abs/10.1680/psm.19164.0034>

- Régnier, J., Cadet, H., & Bard, P.-Y. (2016). Empirical Quantification of the Impact of Nonlinear Soil Behavior on Site Response. *Bulletin of the Seismological Society of America*, 106(4), 1710–1719.
- Régnier, J., Cadet, H., Bonilla, L. F., Bertand, E., & Semblat, J. F. (2013). Assessing nonlinear behavior of soil in seismic site response: Statistical analysis on KiK-net strong motion data. *Bulletin of the Seismological Society of America*, 103(3), 1750–1770.
- Robitaille, B., Marcos, B., Veillette, M., & Payre, G. (1996). Modified quasi-Newton methods for training neural networks. *Computers & Chemical Engineering*, 20(9), 1133–1140.
- Tokimatsu, K., & Midorikawa, S. (1981). *Nonlinear soil properties estimated from strong motion accelerograms*.
- Yu, G., Anderson, J. G., & Siddharthan, R. A. J. (1993). On the characteristics of nonlinear soil response. *Bulletin of the Seismological Society of America*, 83(1), 218–244.
- Zeghal, M., & Elgamal, A.-W. (1994). Analysis of site liquefaction using earthquake records. *Journal of Geotechnical Engineering*, 120(6), 996–1017.